Title

The Co-Optimization of Sustainable Aviation Fuel: Cost, Emissions, and Performance

Authors

Feldhausen, John J

Bell, David C

Kosir, Shane T

et al.

Publication Date

2021-01-11

DOI

10.2514/6.2021-2029

Peer reviewed

The Co-Optimization of Sustainable Aviation Fuel: Cost, Emissions, and Performance

John Feldhausen[1], David C. Bell[2], Shane Kosir[3], and Joshua Heyne[4]
University of Dayton, Dayton, OH, 45409, USA

Corinne Scown[5], Vi Rapp[6], and Ana Comesana[7]
Lawrence Berkeley National Labs, Berkeley, CA, 94720, USA

The combustion of petroleum-based fuels contributes to increases in atmospheric CO_2, contributing to climate change. As other sectors electrify, current battery technology makes this impractical for the aviation industry. The fastest pathway to reducing the carbon contributions of aviation is to create low or no net carbon-emitting drop-in petroleum alternatives. This research explores 3 potential sorghum derived jet fuel molecules from 4 different production routes, hydro-processed esters and fatty acids (HEFA), and Jet A, to identify how blends including these fuels could offer improved performance (MJ/kg, MJ/L) and improved emissions (gCO2/MJ) while minimizing costs. Different applications will value each target metric differently. This research utilizes the Jet Fuel Blend Optimizer (JudO) to create a 4-dimensional Pareto front across potential solutions. The molecules considered will not offer reduced cost compared to conventional jet fuel (Jet A), but they can be utilized to create blends with higher specific energy, greater energy density, and reduced greenhouse gas emissions. Considerations including carbon credits, the sale of byproducts, and the valuation of improved performance will make the proposed molecules more commercially viable. At the lowest region of GHG solutions, coupled with equivalent LCFS approximations, JudO determined blends that could achieve as high as 69% overall carbon reductions at a premium of $0.34/L.

I. Nomenclature

MSP	=	Minimum Selling Price
GHG	=	Greenhouse Gas
LBNL	=	Lawrence Berkeley National Lab
TY-NA	=	Theoretical Yield without Aromatic Constraint
TY-A	=	Theoretical Yield with Aromatic Constraint
JudO	=	Jet Fuel Blend Optimizer
HEFA	=	Hydro processed Esters and Fatty Acids
HPFs	=	High Performance Fuels
MIDACO	=	Mixed Integer Distributed Ant Colony Optimization

[1] Graduate Research Assistant, Mech. & Aero. Eng., non-member
[2] Graduate Research Assistant, Mech. & Aero. Eng., non-member
[3] Graduate Research Assistant, Mech. & Aero. Eng., AIAA Student member
[4] Associate Professor, Mech. & Aero. Eng., AIAA Member
[5] Staff Scientist, non- member
[6] Research Scientist, non-member
[7] Scientific Engineering Associate, non-member

II. Introduction

The current aviation sector occupies roughly 2% of all anthropogenic CO_2 emissions [1], and the International Air Transport Association (IATA) suggests that air travel will double over the next two decades [2]. Consequently, emissions are predicted to rise at a proportionally increased rate unless technological breakthroughs respond. With the rising acceptance and adoption of renewable energy in other applications along with the electrification of the automotive industry, the aviation sector will likely grow to hold an appreciable share of global anthropogenic CO_2 emissions. Motivated to resolve aviation's climate impact, focus has been placed on reduced-emissions fuel production pathways. These pathways consider every emission event that the fuel goes through from feedstock to function [3]. In a recent lifecycle analysis of greenhouse gases (GHG), De Jong et al. reports that it is possible to achieve significant emission reductions with new sustainable aviation fuels (SAFs) [4]. However, the minimum selling points (MSP) of these fuels currently make them undesirable as an alternative to the existing conventional jet fuel options. This study will provide a monetary and emissions reduction context, all in relation to the overarching operability limits and fuel performance.

As shown in the previous research [3], both cost and emissions are highly sensitive to the yield scenario being considered; therefore, this optimization study will be incorporating all three of the scenarios, which will provide greater resolution to the differences among each consideration. Specifically, current yield (CY), baseline yield (BY) which represents 50% of theoretical stoichiometric yield, and theoretical yield (TY) which represents 100% of theoretical stoichiometric yield. Furthermore, these three scenarios will be run at two unique settings with the aromatic constraint and without the aromatic constraint outlined in ASTM 7566 [5]. Previous research [6] determined the performance benefits that are available through the removal of the aromatic constraints. This paper will build on this by analyzing the impact of aromatic removal while considering the aforementioned yield scenarios. Additionally, material compatibility studies [7,8] suggest that sufficient O-ring volume swell is attainable via cycloalkanes as opposed to aromatics. Therefore, the replacement of aromatics with cycloalkanes can increase fuel performance while remaining within the boundaries of material compatibility.

One pathway to improve the financial viability of sustainable fuels is to engineer drop-in high-performance fuels (HPFs) that achieve greater energy intensities while remaining within the operability and safety standard limits outlined in ASTM D7566 [5]. By blending molecules at optimized ratios, the HPFs can exceed the cost-benefit threshold established by other SAFs by offering increased flight payload, increased aircraft range, and greater revenue potential through reduced fuel per flight [6]. Figure 1 depicts the categories needed for compatibility and safety (yellow to red colormap) and performance and value (green colormap), main factors considered for each biomass-derived fuel from the performance, safety, and operability standpoint. Specifically, the yellow-red region highlights the operability and safety requirements that a blend must satisfy to qualify as a 'drop-in' fuel. In contrast, the green highlights the opportunities for performance improvement and value addition. This figure captures the various considerations that have previously been incorporated into JudO. This study will expand that functionality to cost and emissions.

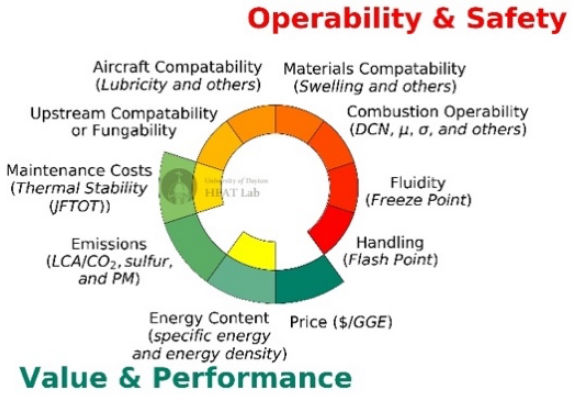

Fig 1: Operability and safety constraints that need to be met for novel SAF approval (yellow-red shading) and opportunities to improve the value and performance of a SAF (green shading).

This study incorporates techno-economic analysis (TEA) and lifecycle analysis (LCA) of greenhouse gas emissions [3] into the Jet Fuel Blend Optimizer (JudO) [6], which will optimize the MSP, GHG emissions, specific energy [MJ/kg] (SE), and energy density [MJ/L] (ED) of the fuel while remaining within operability and safety limits. With the functionality of JudO, neat molecule performance can be enhanced beyond the equivalent potential of the

isolated neat molecules or fuels, and this study will deliver these optimum values, or Pareto front points, along with the anticipated GHG emissions and MSP associated. Optimization will combine both the neat molecules from the literature [3], hydro-processed esters and fatty acids (HEFA) [9], and conventional jet fuel (Jet A).

III. Material

The biologically-produced molecule pool in this study was comprised of monoterpenes and sesquiterpenes. The monoterpene pathways (C10 isoprenoids) included: limonene to limonane, 1,8 cineole to limonane, and linalool to RJ-4. Additionally, a sesquiterpene (C15 isoprenoid) pathway was considered in bisabolane. Each molecule was modeled based on use of a biomass sorghum feedstock, pretreated with an ionic liquid, cholinium lysinate, and saccharified using a cocktail of enzymes to produce what is known as the hydrolysate. Each molecule can be biologically produced from any conventional or cellulosic sugar source. Beyond the previously described molecules, two other fuels were added into the selection pool: Jet A (A-2, POSF 10325) and approved renewable jet fuel, HEFA (POSF 6152). Both of these fuels help the blend initializer satisfy the operability limits that are outlined in ASTM 7566 [5]. If considering the set of optimization runs that uphold the ASTM 7566 minimum aromatic requirement, Jet A significantly contributes to these blends because it is the only source of aromatics. Therefore, in order to meet the constraint, each of these aromatic runs will include a minimum of 47% Jet A. However, HEFA was included because it has already been approved in blends up to 50% [10] and exhibits high-performance characteristics and promising life-cycle emissions at 27 gCO_2/ MJ [4].

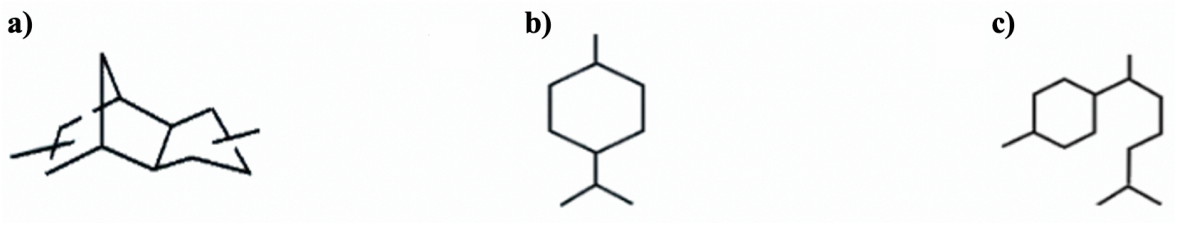

Fig 2: The molecular structures of a) RJ-4 b) limonane and c) bisabolane.

The Jet A properties came from the National Jet Fuel Combustion Program [11], and the GHG and MSP benchmark values were defined in the literature [3][12]. Used cooking oil was taken as the HEFA feedstock because it offered the lowest emission values of the available feedstock options. The MSP values came from the literature [13], and the GHG values were provided by lifecycle analysis that was conducted in literature [4]. Assuming carbon neutrality, the sorghum-derived biofuels and HEFA emission values do not consider combustion due to the sequestered carbon during the life of the biomass. Conversely, this explains why emissions due to combusition has been included for Jet A. The remaining HEFA operability properties came from an online AJF database [14].

Beyond the scope of GHG and MSP values, it was important to define each of the operability properties that characterize the neat molecule/fuel blends to ensure that the Pareto front solutions represent 'drop-in' fuels. The majority of the properties for this study came from the NIST Web Thermo Tables [15], which offers a wide variety of properties at the desired temperatures outlined in ASTM 7566. The remaining values were gathered from the literature and through extrapolation [16]. An overview of the sources, values, and computational paths are provided in the appendix in Table 4a and 4b. The objective values for each of the considered molecules and fuels are summarized below in Table 1.

Table 1: Properties of neat molecules and fuels used in this study.

			Current Yield		**Baseline Yield**		**Theoretical Yield**	
	SE	ED	GHG	MSP	GHG	MSP	GHG	MSP
Molecule/Fuel	*MJ/kg*	*MJ/L*	*gCO_2/MJ*	*$/L-Jet A*	*gCO_2/MJ*	*$/L-Jet A*	*gCO_2/MJ*	*$/L-Jet A*
Bisabolane	43.76	35.99	124.3	6.2	89.8	4.42	48.9	2.29
P-Menthane 18	43.41	34.89	139.8	6.4	83.3	3.84	47.3	2.10
P-Menthane H	43.41	34.89	219.1	10.6	85.5	4.04	46.9	2.09
RJ-4	42.59	39.19	298.3	14.38	89.6	4.50	51.1	2.62
HEFA- UCO	43.90	33.00	27.0	1.04	-	-	-	-
Jet-A	43.06	34.577	87.5	0.61	-	-	-	-

IV. Methods

The general JudO methodology can be grouped into four main sections: (1) randomization of mole fractions over a specified number of iterations and checking that the compiled blend satisfies the operability and safety limits (2) performing optimizations based on 1000 initial guesses (3) combining all separate MIDACO solutions into one data frame, and (4) determining the cumulative 4D Pareto front. Below in Table 2, the constraints and optimization scenarios are detailed. It should be noted that each aromatic or non-aromatic scenario includes three yield settings: current, baseline, and theoretical.

Table 2: Summary of objective functions and constraints for each optimization scenario.

Scenario	Additional Constraints	Optimization Objectives	Mutual Constraints
Aromatic	Aromatic % by Volume	Specific Energy, Energy Density, GHG Emissions, MSP	Viscosity at -20°C, Viscosity at -40°C, Flash Point, Freezing Point, Density at 15°C, DCN
No Aromatic	None		

In recent applications [6,8,17], JudO incorporated a robust convergence evaluation which was conducted after finding the initial set of solutions. This was employed in the form of revision rounds where the mole fractions of solutions along the discontinuous portions of the Pareto front served as initializations for the upcoming rounds. However, due to the number of run scenarios being considered in this study and the computational cost associated with the four-dimensional Pareto front, the revision rounds were removed from this study. This study will include 1000 initial guesses and will be run similar to the first round of the material compatibility JudO study [8].

A. Randomization

To explore the entirety of the solution space in an unbiased manner, the mole fractions of the fuels and molecules were randomized. The process of doing so included three main sections: (1) randomly selecting the molecule before assignment, (2) generating a non-biased value for that assignment, (3) and normalizing each of the mole fractions such that they summed to one. After generating the mole fractions for each of the molecules, the equivalent blended properties were generated through the blend rules from literature [18], and randomizations were checked via the operability limits outlined in ASTM 7566. Additionally, the reproducibility factors outlined in the ASTM 7566 were incorporated to add a factor of safety. Taken together, the randomization and evaluations comprised the optimization precursor of the methodology. Lastly, it should be noted that considering only at the sorghum bio-derived molecules (i.e., bisabolane, limonane, and RJ-4), there exists no combination that satisfies the operability constraints. To better understand the failure rates, and which properties were causing the most failures, a case study of 50,000 randomized mole fractions with the only biomass molecules was considered. The results showed that the melting point failed at 76%, DCN at 61 %, and low-temperature viscosity at 54%. These failures led to the inclusion of Jet A and HEFA for all optimizations in this study which raised the overall success rate from 0% to 17.9%. This would indicate that 82.1% of all randomized blends do not meet the operability requirements even when including Jet A and HEFA.

B. MIDACO

The workhorse of JudO involves Mixed Integer Distributed Ant Colony Optimization (MIDACO), which was employed to determine the minimum GHG emissions, minimum selling price, and maximum SE, and maximum ED values. MIDACO was selected because of its performance with nonlinear benchmark problems [19], low computational cost, and its proven success with blending molecules across different applications [8,17,18]. Identical parameters from previous literature were employed in this study [18]. The main difference from previous studies is in the handling of the bulk solutions returned by MIDACO and the identification of the four-dimensional Pareto front as opposed to the two-dimensional Pareto front.

C. Four-Dimensional Pareto Front Extraction

The four-dimensional Pareto front is defined as a surface of solutions that are non-dominated, representing the optimal solutions from the solution space. Due to time restrictions, the time to process the entire solution space generated by the 1000 initializations was not feasible. Therefore, the solution space was reduced by selecting every

10^{th} point and determining the equivalent Pareto front from these solutions, letting them serve as a representation of the full solution space.

D. Viscosity and Density Extrapolation

Before evaluating the blends at random mole fractions, it was essential to have each of the molecules and fuels defined at the critical temperatures. For this study, the kinematic viscosities were required at -20°C and -40°C, and therefore needed to be extrapolated to meet these requirements if they were unavailable at these temperatures in the literature. The extrapolation procedure followed the work that was outlined in the literature [6], which aligns with the ASTM D341 procedure [16]. Similarly, the densities for each material considered were required at -20°C, -40°C, and 15°C. These were found through performing a standard linear extrapolation.

E. GHG and MSP Blending

The blending rules for the GHG and the MSP each follow a linear by volume fraction format as depicted in Eq. 1 and Eq. 2. Volume fractions were chosen due to the industry convention of the sale price per unit volume.

$$\sum_{i}^{N} \phi_i \mathrm{GHG}_i \qquad \text{Eq. 1}$$

$$\sum_{i}^{N} \phi_i MSP_i \qquad \text{Eq. 2}$$

F. T_{10} Distillation Blending

Distillate properties of jet fuel are included as requirements in ASTM D1655. The distillation curve of a fuel acts as a proxy for molecular weight distribution within a fuel. In this research, because the fuels are neat fuels, the blends will result in unconventional distillation curve behavior. In this research, T10 was not included as a constraint. The final boiling point constraint requiring the final boiling point to be under 300°C will always be satisfied for these fuels because they each have final boiling points below the max allowable.

G. Aromatic Constraint

Current jet fuel specifications [5] require a greater than 8% concentration of aromatics by volume; however, none of the sorghum candidates contain any aromatics. Aromatics are required for their contributions to O-ring volume swell, but generally speaking, they are undesirable because of their low specific energy and high sooting propensity. Research has shown that cycloparaffins likely provide material compatibility similar to aromatics, which would allow for the lower aromatics limit to be dropped in fuels with high concentrations of cycloparaffins [8]. The SAF candidates in this paper are all cycloparaffins. Because all blends of these fuels possible would likely satisfy the O-ring swell either via the aromatics in Jet A or the cycloparaffins from the SAF candidates, solutions were explored with and without the aromatic constraint

V. Results and Discussion

The results of the statistical analysis across the optimization scenarios are outlined below in Table 3. The findings in this table provide a glimpse of the overall solution space found across each optimization scenario. The first key difference between the two main groups can be explained by the increased mole fraction occupied by Jet A within the aromatic blend solutions. Specifically, the Jet A median mole fraction values for the aromatic group were 0.75, 0.68, and 0.73 for the current yield, baseline yield, and theoretical yield, respectively, while the non-aromatic group had median mole fractions of 0.40, 0.23, and 0.28. Due to the aromatic constraint, the minimum Jet A mole fractions were .55, .54, and .54 versus the non-aromatic group where Pareto solutions were found with 0% Jet A. Because Jet A occupies such a significant portion of these mixtures, the results are significantly driven by the Jet A properties which were outlined earlier in Table 1.

Specific energy and energy density values follow similar increasing trends when comparing mean values of the aromatic yield scenarios to their respective non-aromatic scenarios. Due to the effect of reduced Jet A in the mixtures, higher energy intensity values are shown across the non-aromatic group because of the increased mole fractions of the bioderived fuels that carry higher energy intensity properties than Jet A. Specifically, the baseline non-aromatic group shows the highest mean value, while the theoretical yield produces the highest energy density of 34.87 MJ/L. The SE

minimum values across each of the groups align due to solutions in both groups with high amounts of RJ-4, which is the only fuel considered with a lower specific energy value than Jet A. Similarly, large HEFA concentration produces similar trends across the ED minimum values across the two groups, regardless of the yield scenario. The exact biofuel compositions and distributions are detailed further in the compositions section of this study.

The driving effort behind this research lies in the mitigation of carbon emissions relative to conventional jet fuel. The GHG statistical analysis of the cumulative Pareto front is detailed in the next section of Table 3. Similar to the energy intensity trends, the mean values across the non-aromatic group exhibit more desirable results than the aromatic group. The maximum boundary across each yield scenario outside of the current yield is equivalent to the current emissions of conventional jet fuel. These high maximum values are supported by the elevated GHG values detailed in Table 1 under the current yield column. Here it is shown that all four sorghum pathways include higher GHG values than the Jet A value of 87.5 gCO_2/MJ. Specifically, the high GHG values are 124.3, 139.8, 219.1, and 298.3 for bisabolane, limonane via 1,8 cineole, limonane via limonene, and RJ-4 respectively. Conversely, the sorghum biofuels each include values beneath the Jet A benchmark at the theoretical yield. The impact of these reductions can be shown by promising minimum GHG values within the TY-NA group. Specifically, GHG reduces 49.1% from CY to TY at values of 63.38 to 31.54 gCO_2/MJ, respectively. This reduction demonstrates the impact of advancements in yield conversion technology. Later sections will explore the economic perspective in depth by applying the Low Carbon Fuel Standard (LCFS) credits to the minimum GHG values across the theoretical non-aromatic (TY-NA) scenario. This will enable approximations of the cost disparity remaining relative to Jet A at \$0.61. This minimum GHG point along the TY-NA scenario will also be explored from a composition and property perspective in upcoming sections.

The final objective variable considered in the Table 3 summary was minimum selling price (MSP). The minimum value shown by the table is \$0.61/L across each optimization scenario because each optimization run included at least one pure Jet A solution. It is important to point out that although pure Jet A exists along the Pareto front, HEFA does not display the same behavior even though it holds the lowest GHG value of 27 gCO2/MJ. This is because pure HEFA does not meet the density operability requirements.

Table 3: Statistical summary of cumulative Pareto fronts across each of the optimization scenarios.

		Aromatic			No Aromatic			
Property		*Current*	*Baseline*	*Theoretical*	*Current*	*Baseline*	*Theoretical*	**Jet - A**
SE, MJ/kg								
	Min	42.99	42.99	42.99	42.99	42.99	43.00	
	Mean	43.22	43.22	43.18	43.31	43.34	43.33	**43.06**
	Max	43.40	43.40	43.40	43.66	43.66	43.66	
ED, MJ/L								
	Min	33.94	34.05	33.94	33.94	33.97	33.95	
	Mean	34.53	35.17	34.71	34.72	34.79	34.87	**34.60**
	Max	35.75	36.60	35.78	36.01	36.02	36.02	
GHG, gCO2/MJ								
	Min	63.36	59.88	61.92	63.38	38.64	31.54	
	Mean	85.75	81.27	74.32	98.23	61.38	51.20	**87.50**
	Max	159.40	87.13	87.50	206.47	87.78	87.50	
MSP, \$/L-Jet A								
	Min	0.61	0.61	0.61	0.61	0.61	0.61	
	Mean	1.39	1.52	0.89	2.98	1.80	1.33	**0.61**
	Max	5.53	2.16	1.37	9.93	3.80	2.13	

A. Pairwise Plotting of Objective Variables

Pairwise plots were implemented to further evaluate the blends across emission, financial, and energy intensity perspectives. The color was included to observe trends across the solution spaces, while the density of the plotted points indicates the number of solutions found at a given coordinate. In addition to the concentration of points, the diagonal region provides the univariate distributions for the corresponding axis. The blue shaded regions of the subplots represent the regions of the Pareto frontier that outperform conventional jet fuel in both axes. Therefore, no blue shaded region exists for the bottom MSP row of plots because none of the Pareto solutions outperform Jet A in that respect. Furthermore, the red dashed lines indicate the benchmark values offered by Jet A.

Figure 3 illustrates the cumulative Pareto front against the color gradient filter of Jet A. As expected, the solution space is highly concentrated with Jet A near the intersection of the red dashed lines and gradually transitions away from that intersection toward lower mole fractions. It is observable in the energy density vs. specific energy plot that lower concentrations of Jet A extend the solution set into the desired region of solutions. As previously mentioned, this is explained by the higher energy intensities associated with the sorghum biofuels. Each of the plots in the bottom row, which consider the minimum selling price illustrates the inverse relationship between Jet A concentration and selling price. Furthermore, when looking at the MSP vs. GHG axis, a clear peak emerges where GHG reaches a minimum value. Also, more information about the lowest GHG region can be deduced from the GHG vs. SE plot. This subplot exhibits a clear inverse relationship between gCO_2/MJ and MJ/kg. In order to confirm the analysis of subplot GHG vs. SE, MSP vs. GHG was plotted with SE as the color gradient in the inset plot located in the top right of Figure 3. This is the minimum TY-NA, GHG value of 31.54 gCO_2/MJ that was discussed earlier in the GHG statistical analysis section. The exact mole fractions at this min point are RJ-4 at .22 and HEFA-UCO at 0.78. Further clarity of these trends can be gathered in the composition plot shown in the next section.

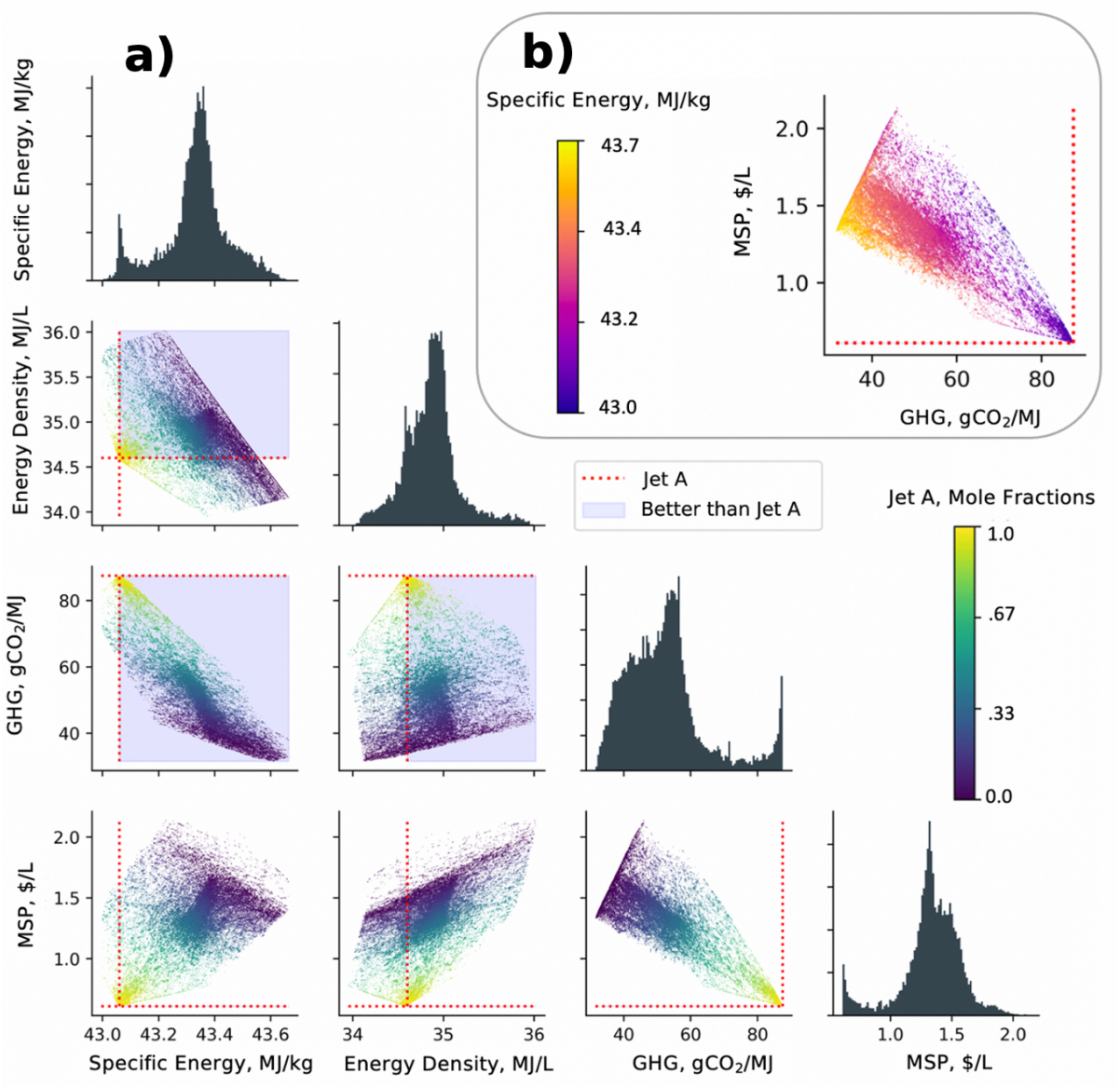

Fig 3: a) Pairwise plot of Jet A mole fractions throughout the TY-NA Pareto frontier, with blue regions representing improvements from Jet A and red lines representing the location of neat Jet A. b) The inset plot contains MSP versus GHG with SE colormap for the TY-NA Pareto front.

B. Composition

The plot shown below provides a visual representation of the composition of each fuel type with respect to the four objective variables. The size of the regions occupied at a given coordinate corresponds to the mole fraction that fuel contributes to that specific blend solution along the cumulative Pareto front. The noise that appears on the boundaries of a selected fuel color derives from the removal of revision rounds from JudO framework and remaining discontinuities existent along the Pareto frontier. These discontinuities also stem from the trimming of the overall MIDACO solution set. With that said, this plot adequately provides a visual representation of the trends present across each of the optimized variables.

The overall trends depicted in these composition plots link to the properties previously detailed in Table 1. Starting with the specific energy plot, a direct relationship between specific energy and HEFA appears, while an indirect relationship is shown for Jet A. The energy density and MSP plots indicate direct relationships with both limonane pathways.. Regardless of the objective variable, low concentrations of bisabolane are observed due to the limiting high viscosity values observed at -40 °C. Summary of all property values are located in the appendix under Table 4a and 4b. Interestingly, the low end of the GHG plot below suggests that blends of HEFA and RJ-4 offer the lowest-emitting pathway, despite RJ-4 being the most emission intensive fuel on its own other than Jet A. However, since the largest GHG reductions are achieved through maximizing HEFA, it is seen that RJ-4 offers a nice compliment from the density perspective enabling the overall blend to meet all operability requirements without the inclusion of Jet A.

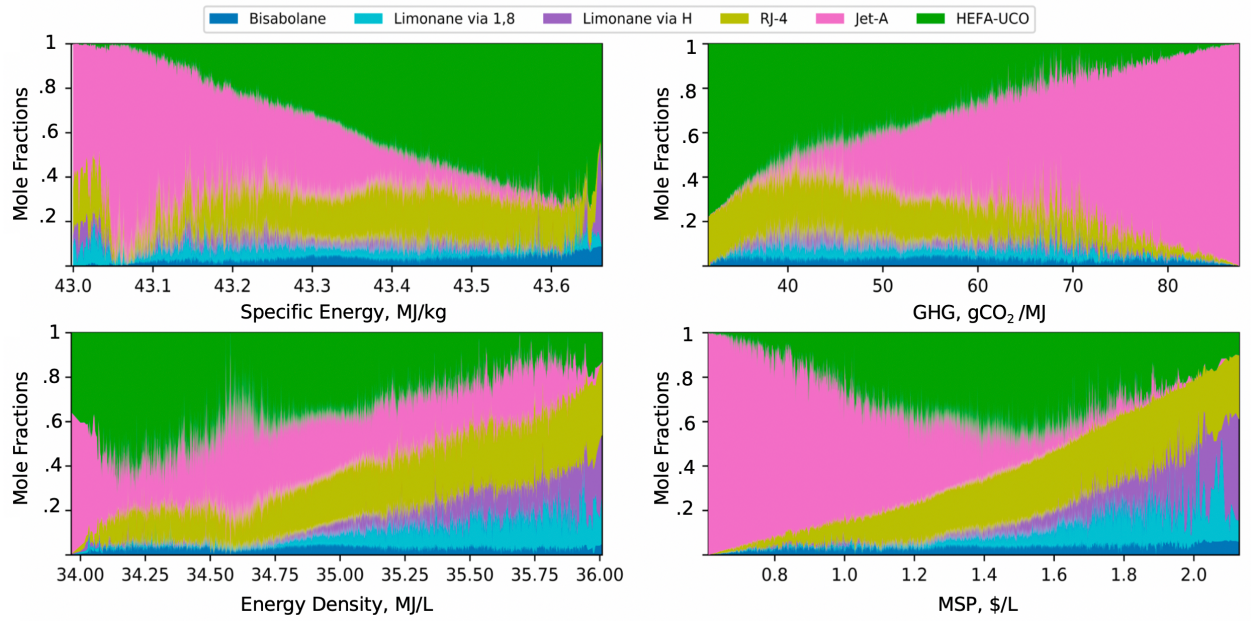

Fig 4: Composition plot for the TY-NA scenario across the four objective variables. These plots were the result of a rolling average of every five points after being sorted with respect to the objective variable shown along the x axis.

Figure 5 illustrates the distributions of each of the four sorghum pathways with respect to the entire Pareto solution population. Specifically, the top subplot considers each blend solution individually as a summation of each of the sorghum derived components and then plots the frequency of those components. In other words, the plot shown on top is the summed distribution of all mole fractions except for the contribution from HEFA or Jet A. From this summed plot, it becomes clear that sorghum fuels combined to hold mole fraction of 0.32 of the overall Pareto blend solution. Each of the means are plotted with red dashed vertical lines. Beneath the summed plot, each of the sorghum derived distributions are shown at their respective scales. Note the variance across the x-axis scaling and the number of solutions occupying this space along the y-axis. Taken together, it is clear that minor contributions come from the limonane pathways, while bisabolane and RJ-4 contribute to more of the Pareto solutions. Altogether, the sorghum contributions to the solution space were much lower than that of Jet A or HEFA.

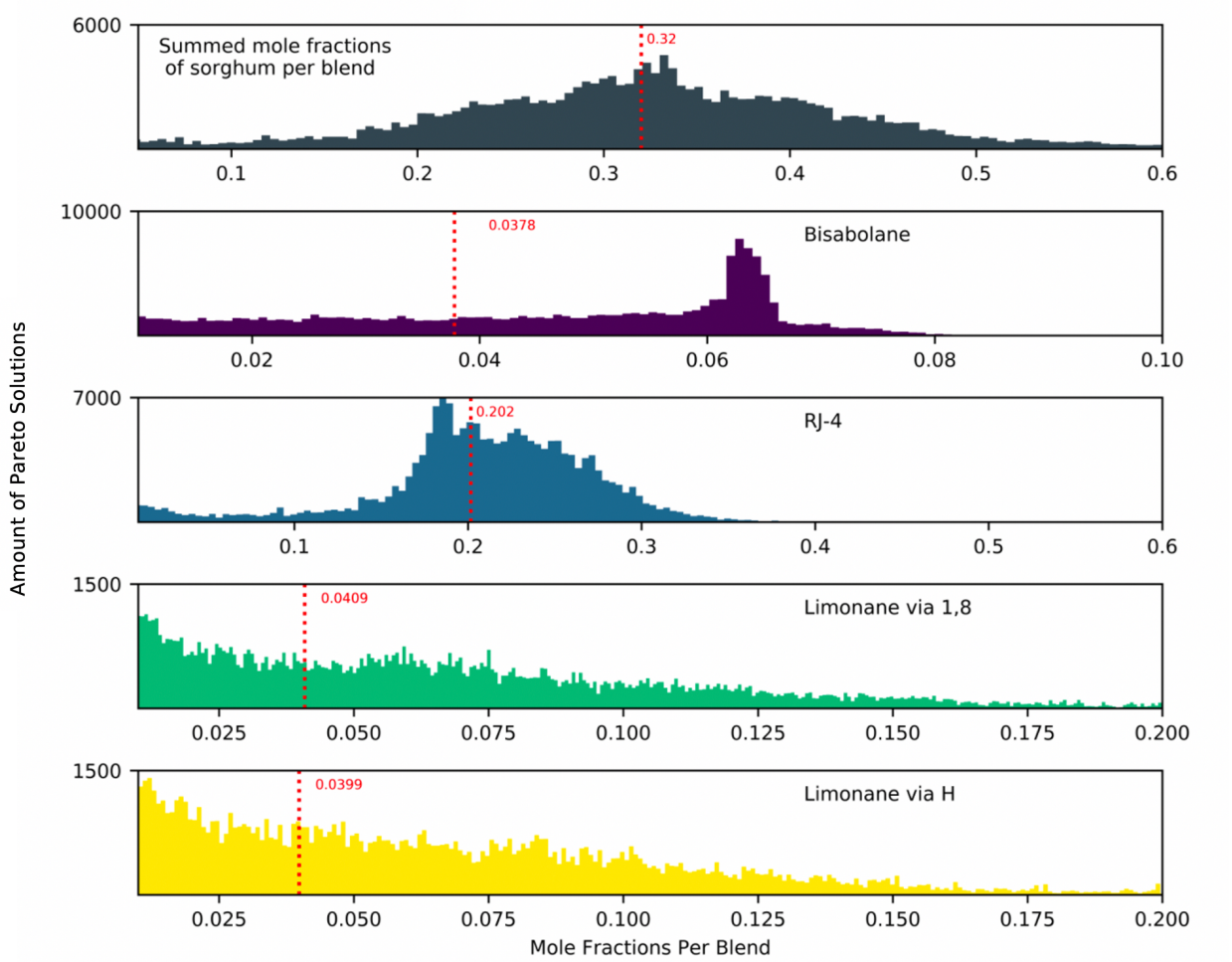

Fig 5: Advanced biofuel mole fraction distributions across the Pareto front for the TY-NA scenario.

C. LCFS Credits

A model was constructed using available LCFS credit prices relative to carbon intensities provided by a recent investment forecast put together by CITI bank [20]. This model was based on the current California LCFS credit price of \$200/MT CO_2 and has been adjusted based on the nominal Jet A carbon intensity value of 87.5 gCO_2 assumed for this study. Considering these assumptions, an approximation was made at the minimum GHG solution for the TY-NA scenario, which demonstrated the adjusted selling price based on the additional revenue that the LCFS credit provides. The resultant LCFS credit price for this minimum solution was computed to 0.38 \$/L under each of the stated assumptions with SE of 43.6 MJ/kg, ED at 34.1 MJ/L, with an MSP of \$1.34/L. Therefore, it was shown that the apparent minimum capable selling price is \$0.96/L for the TY-NA minimum GHG fuel. At this mark, carbon reductions of 63.9% from conventional jet fuel are achieved along with a performance boost of 1.39 % for SE, and for only a \$0.34/L added premium. Performance benefits associated with increased SE and ED would allow for additional revenue generation. It should be noted that the values stated above apply to a single solution found on the Pareto front.

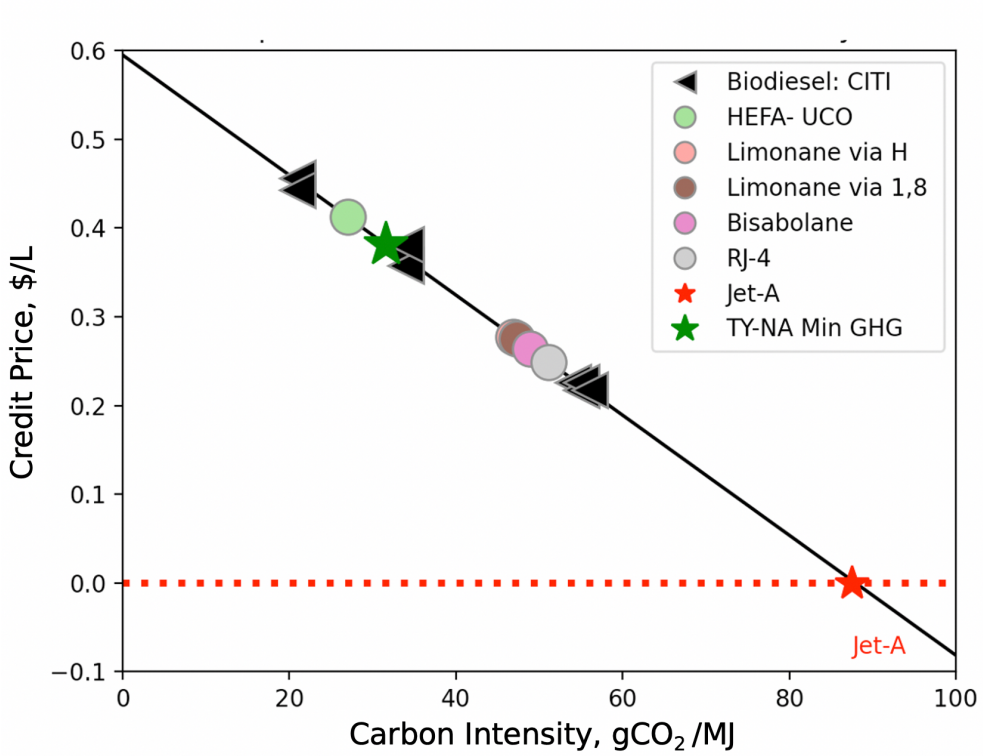

Fig 6: Linear model of LCFS credit price versus carbon intensity.

VI. Conclusion

The results of this study demonstrate the performance benefits conferred via the addition of biofuels, despite the limited selection pool of molecules and tight constraints enforced by ASTM 7566. At the low boundary of the GHG solutions, coupled with equivalent LCFS approximations, JudO determined a blend that could achieve as high as 69% overall carbon reduction at a premium of $0.34/L. Future research seeks to incorporate more added value streams to further approximate the economics of implementing biofuels across the entire Pareto frontier. Value added from increased energy intensity, value added from different co- products such as lignin, and value added from LCFS credits will be captured beneath one optimization function written in terms of cost per flight. Consideration will also extend to thermal stability benefits. Additionally, the upcoming efforts will incorporate the revision rounds to achieve higher levels of convergence and confidence in the cumulative Pareto front. Furthermore, optical dilatometry will be included to demonstrate that the removal of the aromatic constraint does not hinder compliance with material compatibility requirements.

Appendix

Table 4a: Summary of properties

Molecule/Fuel	Aromatic *% vol*	Freezing Point *°C*	Flash Point *°C*	Boiling Point *°C*	DCN	HC	MW *g/mol*
Bisabolane	0	-6.7 [21]	111 [22]	256.85 [15]	41.9**Error! Bookmark not defined.** [23]**Error! Bookmark not defined.**	2.0	210
Limonane	0	-87.6 [24]	45.1 [25]	146.09 [15]	29.10 [26]	2.0	140
RJ-4	0	-40.2 [27]	72.45 [27]	220.85 [27]	23.50 [26]	1.7	164
HEFA-UCO	0	-77.0 [14]	43.00 [14]	259.00 [14]	58.30 [14]	2.7	161
Jet A	0.17 [11]	-51.0 [11]	48.00 [11]	270.00 [11]	48.30 [11]	1.9	159

Table 4b: Summary of properties

Molecule/Fuel	η (-20 °C) mm^2/s	η (-40 °C) mm^2/s	ρ (-20°C) kg/m^3	ρ (-40°C) kg/m^3	ρ (15°C) kg/m^3
Bisabolane	20.031‡	79.9‡	0.859*	0.879*	0.822*
Limonane	2.051‡	2.81‡	0.825*	0.837*	0.804 [15]
RJ-4	18.741‡	60.0 [28]	0.927*	0.931 [28]	0.920*
HEFA-UCO	3.3 [14]	6.4 [14]	0.776 [14]	0.793 [14]	0.751 [14]
Jet A	4.5 [11]	9.1 [11]	0.829 [11]	0.833 [11]	0.803 [11]

‡ Extrapolation through ASTM D341 [16]
* Linear extrapolation by mole fractions

Acknowledgments

The authors would like to thank the Sandia National Labs for sponsoring this work (PO# 2110793).

References

[1] IATA - Climate Change. https://www.iata.org/en/policy/environment/climate-change/. Accessed May 28, 2020.

[2] IATA - IATA Forecast Predicts 8.2 Billion Air Travelers in 2037. https://www.iata.org/en/pressroom/pr/2018-10-24-02/. Accessed May 28, 2020.

[3] Baral, N. R., Kavvada, O., Mendez-Perez, D., Mukhopadhyay, A., Lee, T. S., Simmons, B. A., and Scown, C. D. "Techno-Economic Analysis and Life-Cycle Greenhouse Gas Mitigation Cost of Five Routes to Bio-Jet Fuel Blendstocks." *Energy and Environmental Science*, Vol. 12, No. 3, 2019, pp. 807–824. https://doi.org/10.1039/c8ee03266a.

[4] De Jong, S., Antonissen, K., Hoefnagels, R., Lonza, L., Wang, M., Faaij, A., and Junginger, M. "Life-Cycle Analysis of Greenhouse Gas Emissions from Renewable Jet Fuel Production." *Biotechnology for Biofuels*, Vol. 10, No. 1, 2017, p. 64. https://doi.org/10.1186/s13068-017-0739-7.

[5] American Society for Testing and Materials International (ASTM International). *ASTM D7566-20a: Standard Specification for Aviation Turbine Fuel Containing Synthesized Hydrocarbons*. 2020.

[6] Kosir, S. T., Heyne, J., Stachler, R., and Hauck, F. "High-Performance Jet Fuel Optimization and Uncertainty Analysis." *Fuel*, 2020.

[7] Graham, J. *Impact of Alternative Jet Fuel and Fuel Blends on Non-Metallic Materials Used in Commercial Aircraft Fuel Systems Continuous Lower Energy, Emissions and Noise (CLEEN) Program*.

[8] Kosir, S., Heyne, J., and Graham, J. "A Machine Learning Framework for Drop-in Volume Swell Characteristics of Sustainable Aviation Fuel." *Fuel*, Vol. 274, No. April, 2020, p. 117832. https://doi.org/10.1016/j.fuel.2020.117832.

[9] Tao, L., Milbrandt, A., Zhang, Y., and Wang, W. C. "Techno-Economic and Resource Analysis of Hydroprocessed Renewable Jet Fuel." *Biotechnology for Biofuels*, Vol. 10, No. 1, 2017, p. 261. https://doi.org/10.1186/s13068-017-0945-3.

[10] Vozka, P., and Kilaz, G. "Impact of HEFA Feedstocks on Fuel Composition and Properties in Blends with Jet A." 2018. https://doi.org/10.1021/acs.energyfuels.8b02787.

[11] Edwards, T. "Reference Jet Fuels for Combustion Testing." *AIAA SciTech Forum - 55th AIAA Aerospace Sciences Meeting*, 2017, pp. 1–58. https://doi.org/10.2514/6.2017-0146.

[12] Wang, W.-C., Tao, L., Markham, J., Zhang, Y., Tan, E., Batan, L., Warner, E., and Biddy, M. *Review of Biojet Fuel Conversion Technologies*. 2016.

[13] Pearlson, M., Wollersheim, C., and Hileman, J. "A Techno-Economic Review of Hydroprocessed Renewable Esters and Fatty Acids for Jet Fuel Production." *Biofuels, Bioproducts and Biorefining*, Vol. 7, No. 1, 2013, pp. 89–96. https://doi.org/10.1002/bbb.1378.

[14] 6152 | AJF:TD | U of I. https://altjetfuels.illinois.edu/documents/article.asp?id=98. Accessed Nov. 15, 2020.

[15] NIST/TRC Web Thermo Tables (WTT): Critically Evaluated Thermophysical Property Data. https://wtt-pro.nist.gov/wtt-pro/. Accessed Nov. 24, 2020.

[16] ASTM. "ASTM D341-17 Standard Practice for Viscosity-Temperature Charts for Liquid Petroleum Products." No. July, 2017, pp. 1–6. https://doi.org/10.1520/D0341-17.2.

[17] Kosir, S. T., Behnke, L., Heyne, J. S., Stachler, R. D., Flora, G., Zabarnick, S., George, A., Landera, A., Bambha, R., Denney, R. K., and Gupta, M. "Improvement in Jet Aircraft Operation with the Use of High-Performance Drop-in Fuels." *AIAA Scitech 2019 Forum*, No. January, 2019, pp. 1–27. https://doi.org/10.2514/6.2019-0993.

[18] Flora, G., Kosir, S., Behnke, L., Stachler, R., Heyne, J., Zabarnick, S., and Gupta, M. Properties Calculator and Optimization for Drop-in Alternative Jet Fuel Blends. 2019.

[19] Schlüter, M., Gerdts, M., and Rückmann, J. J. "A Numerical Study of MIDACO on 100 MINLP Benchmarks." *Optimization*, Vol. 61, No. 7, 2012, pp. 873–900. https://doi.org/10.1080/02331934.2012.668545.

[20] CITI. *Selected Low Carbon Fuels Themes Strictly Private and Confidential COVID- 19 Has Been a Test Case of Lower Fuel Demand …*. 2020.

[21] ChemSpider | Search and Share Chemistry. http://www.chemspider.com/Default.aspx. Accessed Nov. 24, 2020.

[22] Pahima, E., Hoz, S., Ben-Tzion, M., and Major, D. T. "Computational Design of Biofuels from Terpenes and Terpenoids." *Sustainable Energy and Fuels*, Vol. 3, No. 2, 2019, pp. 457–466. https://doi.org/10.1039/c8se00390d.

[23] Peralta-Yahya, P. P., Ouellet, M., Chan, R., Mukhopadhyay, A., Keasling, J. D., and Lee, T. S. "Identification and Microbial Production of a Terpene-Based Advanced Biofuel." *Nature Communications*, Vol. 2, No. 1, 2011. https://doi.org/10.1038/ncomms1494.

[24] Data Source Search | Jean-Claude Bradley Open Melting Point Dataset. http://www.chemspider.com/Search.aspx?dsn=Jean-Claude+Bradley+Open+Melting+Point+Dataset. Accessed Nov. 26, 2020.

[25] CompTox Chemicals Dashboard. https://comptox.epa.gov/dashboard/dsstoxdb/results?search=DTXSID9025530. Accessed Nov. 26, 2020.

[26] Harvey, B. G., Merriman, W. W., and Koontz, T. A. "High-Density Renewable Diesel and Jet Fuels Prepared from Multicyclic Sesquiterpanes and a 1-Hexene-Derived Synthetic Paraffinic Kerosene." *Energy and Fuels*, Vol. 29, No. 4, 2015, pp. 2431–2436. https://doi.org/10.1021/ef5027746.

[27] Osmont, A., Gökalp, I., and Catoire, L. "Evaluating Missile Fuels." *Propellants, Explosives, Pyrotechnics*, Vol. 31, No. 5, 2006, pp. 343–354. https://doi.org/10.1002/prep.200600043.

[28] Martel, C. R. "O ~ FILE Cop." 1987.